Dibennardo *et al.*
Translational Medicine Communications (2024) 9:14
https://doi.org/10.1186/s41231-024-00172-0

Translational Medicine Communications

RESEARCH

Open Access

Bioimpedance based biomarker for the detection of precancerous and cancerous lesions of the pancreas: feasibility animal study

Federica Dibennardo[1], Onur Fidaner[1], Les Bogdanowicz[1], Daniel S. Gehrke[1], Donato Ceres[1], Margaret C. John[1], Constantine H. Bovalis[1], Erik M. Kundro[1], Alexander Grycuk[1], Karla Castellanos[2], Adonis Coleman[2], Kavya Sudhir[2], Jorge Heneche[2], Jose Acebedo[2], Angel Jimenez[2], Isaac Raijman[3], Paul Grippo[2] and Martina Guidetti[1*]

Abstract

Background Pancreatic cancer (PC) remains a significant healthcare challenge due to its aggressive nature and poor prognosis. The current gold standard that combines imaging modalities, endoscopy, and biopsies has limited diagnostic efficacy due to various shortcomings.

Methods We propose a feasibility study for the use of a bioimpedance biomarker to detect PC. The biomarker was evaluated in a double blind study on ex vivo pancreata of mice: 15 LSL-Kras^{G12D}; LSL-p53^{R172H}; Pdx1-Cre, 2 LSL-Kras^{G12D}, and 9 wild type controls (Study 1). To determine if the biomarker can distinguish between PC and acute pancreatitis (AP), we challenged it with 18 cerulein-induced AP and 6 saline-injected controls (Study 2).

Results The results from Study 1 showed 100% specificity and 94% sensitivity against histopathology outcomes; for Study 2 all AP and saline-injected pancreases were diagnosed as non-cancerous. Regression analysis revealed a positive correlation between biomarker and pathologically analyzed cancer-induced fibrosis (r(24)= 0.73 (p<0.001)).

Conclusion These findings demonstrate the potential of this bioimpedance biomarker as a diagnostic tool for PC.

Keywords Bioimpedance biomarker, KPC model, Pancreatic cancer detection, Cole relaxation frequency

Introduction

Pancreatic cancer (PC) poses a significant healthcare challenge, accounting for half a million new cases and 4.7% of the world's cancer-related deaths in 2020 [1]. It is notorious for its aggressive nature and poor prognosis, boasting the lowest survival rate among all known cancers according to the American Cancer Society [2–5]. This dismal outcome is primarily due to the challenges in early diagnosis and the absence of standardized guidelines for assessing suspicious pancreatic masses [6, 7]. The intricate pathophysiology of PC, coupled with the lack of early diagnostic and prognostic markers,

*Correspondence:
Martina Guidetti
martina.guidetti.92@gmail.com
[1] NovaScan Inc, 1623 W. Fulton Street, Chicago 60612, IL, USA
[2] University of Illinois at Chicago, 818 South Wolcott Avenue, Chicago 60612, IL, USA
[3] Texas International Endoscopy Center, 6620 Main St STE 1500, Houston 77030, TX, USA

contributes to late-stage diagnoses, often rendering treatment options limited and ineffective.

Presently, there is no established screening procedure for the early detection of PC. Existing imaging and endoscopic modalities, such as multidetector computed tomography (MDCT), magnetic resonance imaging (MRI), endoscopic retrograde cholangiopancreatography (ERCP), endoscopic ultrasound (EUS) [3, 8–11], and quantitative-elastography endoscopic ultrasound (QE-EUS) [12–14], have limitations in accurately detecting small lesions (under 3 cm) and distinguishing between malignant and benign masses [15]. There is demand for an on-site, real-time assessment device that works as a quantitative decision support tool for the endoscopist. A more timely and accurate diagnosis of PC would reduce revisits, expedite treatment, and improve the current prognosis of this disease. Although MDCT is commonly used for PC diagnosis, its reliance on iodine-based contrast agents and exposure to radiation poses risks [10]. MRI is often used as a subsequent test when there is a high suspicion of PC despite a clear CT [10]. However, both CT and MRI are not very sensitive in detecting the tumor in its initial development while still small [15] (typically less than 3 cm) and localized [5]. ERCP, while useful for biliary and pancreatic duct brushing cytology, is predominantly therapeutic due to associated complications [16–18]. EUS-guided tissue acquisition via fine-needle aspiration (FNA) or fine needle biopsy (FNB), the gold standard for sampling pancreatic masses, faces challenges in lesion localization and obtaining representative samples [9, 10, 19, 20].

Advancements in fine needle biopsy (FNB) technologies and elastography have improved the diagnostic yield of EUS, particularly for lesions smaller than 2 cm [5, 10, 21–23]. Elastography assesses tissue stiffness by converting different elasticity values to colors superimposed onto the conventional gray-scale EUS image. Nonetheless, the accurate selection of a representative area from the lesion is crucial for the effectiveness of QE-EUS [12]. Despite these modalities' utility, confirmation of cancerous lesions relies on a cytopathologist's ex vivo biopsy sample analysis, typically performed at an advanced disease stage, which limits curative interventions [19, 20]. Challenges in biopsy procedures stem from difficulty in lesion localization, inter-observer variability, and low diagnostic yield. Additionally, misdiagnosis of tissues may result from pancreatitis, necrosis, or diffusely infiltrating carcinoma [19, 20, 24]. Given the limitations of current diagnostic approaches, research endeavors aim to enhance PC diagnosis. Some focus on real-time assessment of biopsy samples for adequacy and viability [25, 26]. While promising, these techniques are hindered by cost, resolution issues, and potential sample modification before pathological assessment [27, 28]. Thus, there is a pressing need for a real-time diagnostic tool that can evaluate cancer presence without altering the sample, reducing laboratory costs and administrative burdens.

This study proposes a novel approach using bioimpedance-based biomarkers, including the Cole Relaxation Frequency (CRF), to detect PC. Building upon previous research demonstrating the efficacy of CRF in detecting cancerous tissues in breast, skin, and lung [29–32], we hypothesize that CRF can also effectively detect PC in the genetically modified KPC and KC mouse models, as well as differentiate PC from acute pancreatitis (AP) and benign tissues. Our hypothesis posits that CRF, as a quantitative biomarker, will exhibit distinct patterns in PC tissues compared to noncancerous tissues. We predict that CRF measurements will correlate with the progression of lesions from precancerous stages to malignancy, particularly in genetically modified KPC and KC mouse models. Furthermore, we anticipate that CRF will demonstrate high specificity and sensitivity in distinguishing PC from AP, a common confounding factor in PC diagnosis.

Our feasibility study aims to assess whether CRF can detect PC and distinguish it from pancreatitis in genetically modified KPC and KC mouse models, an acute pancreatitis mouse model, and wild-type controls. KPC mice spontaneously and progressively develop PC, allowing us to correlate the biomarker values with the lesions as they develop from precancerous to malignancy. KPC mice, in particular, offer insights into PC progression, mirroring human PC development [33–35]. By evaluating CRF in a double-blind study on ex vivo mouse pancreases, we compare CRF-based cancer determinations against histopathology outcomes to determine specificity and sensitivity. Our aim is to lay the foundation for CRF as a potential diagnostic tool for PC, offering improved accuracy, efficiency, and timeliness compared to existing methods. Unlike traditional histopathology assessment of biopsy samples, NovaScan technology would provide an automatic, non-subjective, and quantitative approach to tissue evaluation. By digitizing the process, it would offer real-time feedback during procedures, serving as a supplementary tool for EUS procedures. NovaScan technology would play a crucial role in ensuring the success of the initial biopsy procedure and facilitating early detection of cancerous conditions.

Methods

Technology background

Several studies have demonstrated that different tissue types and cell behaviors, including cancer, can be identified by measuring frequency dependent bioelectrical properties [29, 30, 36–43]. The cell membrane

behaves like an electrical capacitor, in that a charge (ion) brought up to the outside of the membrane causes charges of the opposite sign to deploy on the interior face of the membrane. This process then stores equal amounts of electrical charge, with opposite signs, on each side of the membrane. However, this charge can be neutralized by charges flowing in the opposite direction through resistive paths between the inside and outside of the cell membrane. Some possible paths are via proteins embedded in the membrane; further paths are possible by a split of the current passing through the cell or around the cell. The behavior of the cell membrane has been described by the circuit diagram (Cole-Cole model). Current passing through the extracellular matrix encounters only resistive impedance to the current flow, as does the current passing through the proteins in the membrane wall with current passing around the cell. A portion of the current also passes through the capacitive membrane, and this has a complex behavior that can be mathematically modeled. The characteristic rate at which a cell redistributes electrical charge on and off the cell membrane, so that the charge gets equilibrated, is called Cole Relaxation Frequency (CRF). By examining the transmembrane cellular response in the frequency range of 1 KHz to 10 MHz, also known as the β region, cancerous tissues can be detected. To characterize spectral bioimpedance measurements, NovaScan has developed an algorithm that utilizes the equivalent circuit proposed by Cole et al. [44]. The circuit is described by the following equation:

$$Z = Z' + jZ'' = R_\infty + \frac{R_0 - R_\infty}{1 + (j\frac{f}{CRF})^\alpha}, \quad (1)$$

where Z is the complex sample impedance, $Z^{'}$ is the real, and $Z^{''}$ is the imaginary component of Z, R_0 and R_∞ respectively represent the low and high frequency limits of Z, f is the measurement frequency, CRF is the Cole Relaxation Frequency, j is the imaginary unit and α is a dimensionless number that is inversely related to the broadening in the frequency domain of $Z^{'}$, and the spread of the peak seen in $Z^{''}$. The algorithm extracts the CRF that is used as an impedance spectroscopy biomarker to detect cancer. NovaScan has established proof-of-concept technologies to detect cancer in breast [29, 45], skin [30], and lung [31, 32] tissues. Moreover, for each type of tissue, NovaScan has developed customized prototype devices that have been tested and validated ex vivo [29–32]. We based the feasibility of the current work on these previous studies and on the work by Subramanian et al., which illustrated cell architecture derangement across tumor formation, further explaining the physical foundation of CRF deviations observed for cancer [46].

Mouse model

Two studies were conducted with a spectral bioimpedance measurement device for CRF biomarker computation to determine if the biomarker could discern between 15 K-ras;Trp53;Pdx-1-Cre (KPC), 2 K-ras;Pdx-1-Cre (KC), and 9 wild type controls and between acute pancreatitis (AP) and PC, by adding to the analysis cerulein-induced AP and saline-injected mice. Histopathological examination confirmed that 12 KPC pancreases were cancerous, 9 controls were noncancerous, and 5 pancreases (3 KPC and 2 KC) showed precancerous conditions with pancreatic intraepithelial neoplasia (PanIN), increasing the precancerous group's sample size to 5. The KPC (LSL-$Kras^{G12D}$/LSL-$p53^{R172H}$/Pdx1-Cre) murine model is a widely used preclinical tool for studying PC. This model involves mutations in both endogenous $Kras^{G12D}$ (K) and $p53^{R172H}$ (P) alleles, along with the Lox-STOP-Lox (LSL) insert, which are simultaneously expressed following Cre (C) induction regulated by the Pdx1 promoter. The phenotypic result triggers the initiation of a high frequency of Pancreatic Intraepithelial Neoplasia (PanIN) lesions that can progress to pancreatic ductal adenocarcinoma (PDAC) [33, 47, 48]. In order to avoid variance in observations from chimeric strains, KPC mice in the B6 strain background develop PanINs at 4-5 weeks, local invasive cancer at 10-12 weeks and more advanced disease at 16-22 weeks, with metastasis in 40% of specimens. The KPC mouse model is among the most commonly used models for studying PDAC due to its faithful recapitulation of human pancreatic cancer biology [33–35, 49, 50]. Studying the prognostic value of CRF with human tissue ex vivo would be challenging due to the extended time required (5-10 years), and it would be nearly impossible in vivo. KPC PDACs provide a unique opportunity to study the evolution of cancer in a controlled setting, not otherwise possible in human patients. KC mice are derived from two separate alleles employing the Cre/Lox system, which is a recombination tool requiring both Cre and Lox-containing genetic components. KC have a Cre allele driven under the Pdx1 promoter (Pdx1 being an early pancreas gene that is essential for gland development; loss thereof results in nonviable mice). The Lox allele was designed with a STOP codon inserted between two Lox sites (LSL), which is essential for Cre-driven recombination resulting in the removal of one Lox site and any intermediate DNA, in this case, the STOP codon. As part of this allele, the mouse Kras locus has been mutated to insert an aspartate in place of glycine at codon 12 (G12D). KC (LSL-KrasG12D/Pdx1-Cre) mice develop neoplastic lesions very similar to human pancreatic intraepithelial neoplasms or PanINs within 1-2 months, and these lesions can progress through stages 1, 2, and 3, with PanIN 3 being a sinister lesion

that can progress to pancreatic cancer [51]. At one year of age or older, about 40% of these KC mice can progress to overt pancreatic cancer with metastatic disease in about 30% [52]. With a long latency, KC mice are not commonly used for pancreatic cancer studies. The addition of a LSL-p53R172H allele to KC mice leads to a recombination event that removes a STOP codon to express a downstream mutant p53 simultaneously with expression of mutant Kras. In these mice, onset of lesions is rapid and progresses to pancreatic cancer typically within 3-5 months; most mice do not live to 6 months of age due to progressive disease [48]. AP was induced through intraperitoneal (IP) injections of 50 $\mu g \cdot kg^{-1}$ cerulein, administered hourly for eight consecutive hours. Eight cerulein IP injections were administered on two alternated days, with a 24 hour period sans injections (Monday= 8 injections, Tuesday= sans injections, Wednesday= 8 injections). Pancreatic tissues were harvested 24 hours, 48 hours and 7 days post the last injection of cerulein according to the 'staggered' protocol. Cerulein control animals received vehicle injections (saline solution, 0.9% NaCl) [53, 54].

Study design and methods

We conducted a double-blind study on ex vivo mouse pancreases to evaluate the biomarker. The initial study involved 15 KPC, 2 KC, and 9 wild type controls, with 12 cancerous, 9 controls and 5 precancerous samples based on histopathology. To assess the biomarker's ability to distinguish between pancreatic cancer (PC) and acute pancreatitis (AP), a secondary study included 18 cerulein-induced AP cases (3 groups at 24, 48, 72 hours, n=6 for each group) along with 6 saline-injected controls. Testing was carried out at multiple locations within the pancreases using a custom-built bioelectrical impedance measurement device equipped with tetrapolar electrodes (Fig. 1). The tetrapolar configuration consists of four electrodes: a source electrode for generating a stimulating high-frequency signal, a drain electrode for measuring current through a precision 50 Ohm shunt resistor, and two pick-up electrodes positioned between the source and drain for measuring the voltage drop across the tissue [31]. This device performed bioelectrical impedance measurements across a frequency range of 1 KHz to 20 MHz. Biological sample measurements were performed using a customized impedance bridge, and resulting signals were digitized and processed by a microcontroller. The bioimpedance biomarker, based on the Cole Relaxation Frequency (CRF), was derived from complex spectral impedance measurements. An electrode array was utilized for tissue sample measurements, fabricated on a printed circuit board with 1x4 mm Ag/AgCl electrode pads spaced 0.5 mm apart. Electrodes were scanned by a motorized XYZ stage controlled by a computer to record impedance at each sample location.

Microscopic evaluation

In this study, Masson's trichrome stain was utilized on pancreas samples to visualize and examine tissue structures, including muscle fibers, cytoplasm, erythrocytes, and keratin (red stain); collagen (blue stain); and nuclei (dark purple stain). The staining process involved microscopic examination of tissue slides and calculating the proportion of fibrotic tissue relative to the total sample area to assess the degree of fibrosis. Subsequently, images of Masson's trichrome-stained of non-cancerous (Fig. 2A-C), pre-cancerous (Fig. 2D-F) and cancerous (Fig. 2G-I) mice pancreases were then captured at a 20x magnification using an Olympus VS200 slide scanner and Aperio AT2 (Leica Biosystems, Buffalo Grove, IL). These images were imported into QuPath, an image analysis software where a pixel classifier tool categorized pixels as background, tissue, or fibrosis (see Fig. 3). The pixel classifications were established based on the manual classification of pixels from a representative region in each image across the entire

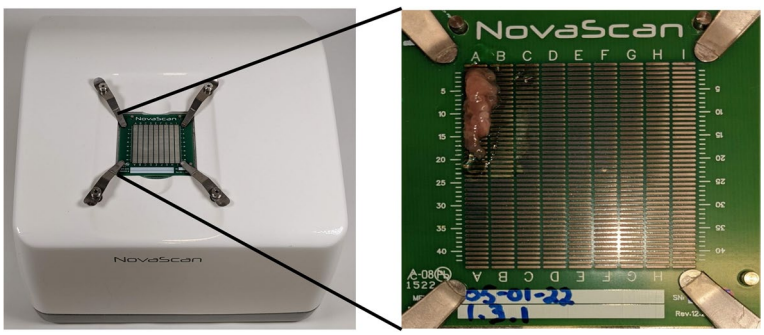

Fig. 1 Bioimpedance spectroscopy measuring device with measurement electrode array used for a series of spectral bioimpedance measurements. A zoom in of the electrode with a pancreas sample is also shown

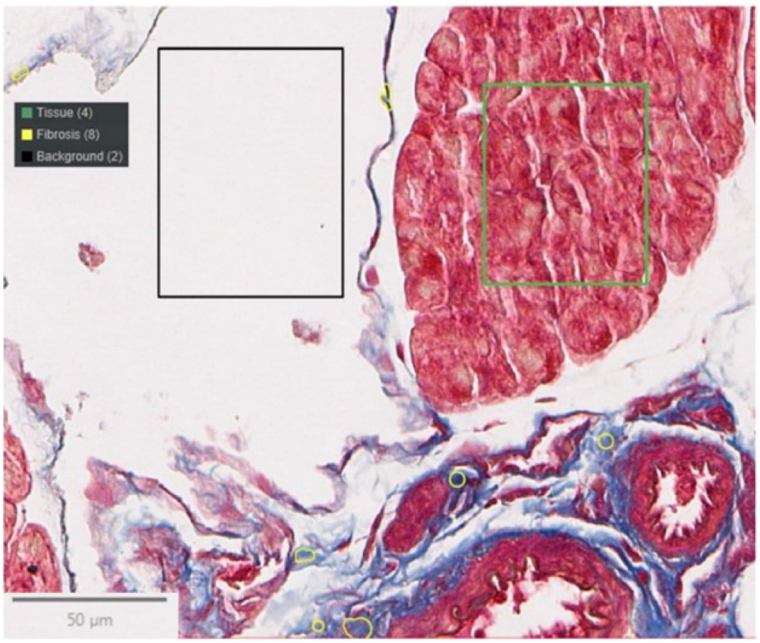

Fig. 2 **A**, **B**, **C** Images of non-cancerous, normal mice pancreas from low to high magnification. The estimation of fibrosis via histological assessment was 0%. Machine learning using QuPath's pixel classifier tool measured fibrosis at 2%. **D**, **E**, **F** Images of pre-cancerous mice pancreas from low to high magnification. A mix of normal fibrotic tissue and lesions with no overt cancer tissue was noted. The estimation of fibrosis via histological assessment was 35%. Machine learning using QuPath's pixel classifier tool measured fibrosis at 11.8%. **G**, **H**, **I** Images of cancerous mice pancreas from low to high magnification. Areas that appear as denser lines of tissue are common artifacts of tissue preparation. A large fibrotic tumor with prominent, well-differentiated ductal carcinoma and lesions with fibrosis was observed on this pancreas. The estimation of fibrosis via histological assessment was 63%. Machine learning using QuPath's pixel classifier tool measured fibrosis at 26.2%

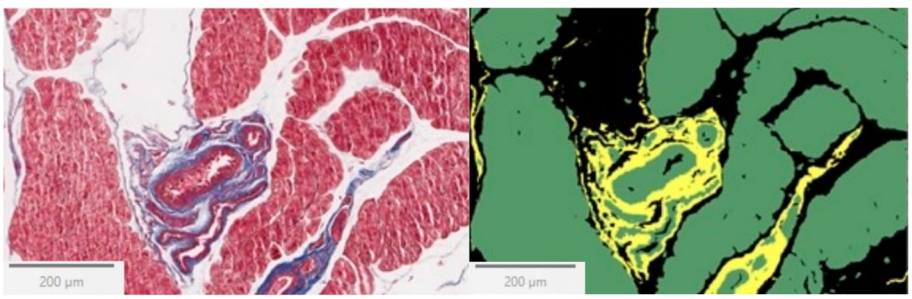

Fig. 3 Annotations drawn on the image are used to train the pixel classifier in QuPath, enabling it to recognize pixels belonging to the background (black), fibrosis (yellow), and tissue classifications (green)

image set. Different settings of the pixel classifier, such as resolution and classifier type, were explored for optimal classification accuracy. Additionally, an overlay of the pixel classifications and the original image was used to assess the classifier's accuracy, to compare manually scored fibrosis estimates to the quantitative values obtained from QuPath (see Fig. 4). To calculate the percentage of fibrosis, pixel area measurements were extracted for each classification, and the fibrosis area was divided by the sum of fibrosis and tissue areas.

Cancer determination was based on a CRF biomarker threshold above 1 MHz (Fig. 5). After bioimpedance testing, all samples underwent standard histopathology processing. Sensitivity and specificity of the bioimpedance biomarker based outcomes were determined against histopathology outcomes as ground truth. During histopathological examination, pancreases were evaluated for percent fibrosis averaged over multiple fields of view. Spearman correlation was used to determine if there was any correlation between percent fibrosis (both estimated

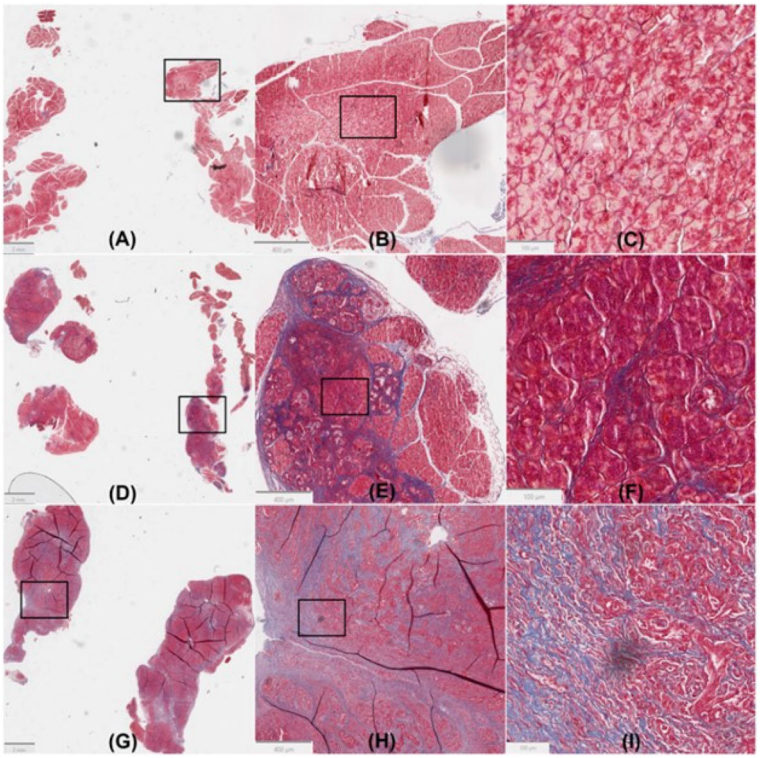

Fig. 4 Visualizing the original image (left) and an overlay of the pixel classifications on the original image (right) was used to gauge the accuracy of the pixel classifier. In the context of the image on the right, the color green represents tissue, yellow represents fibrosis, and black represents the background

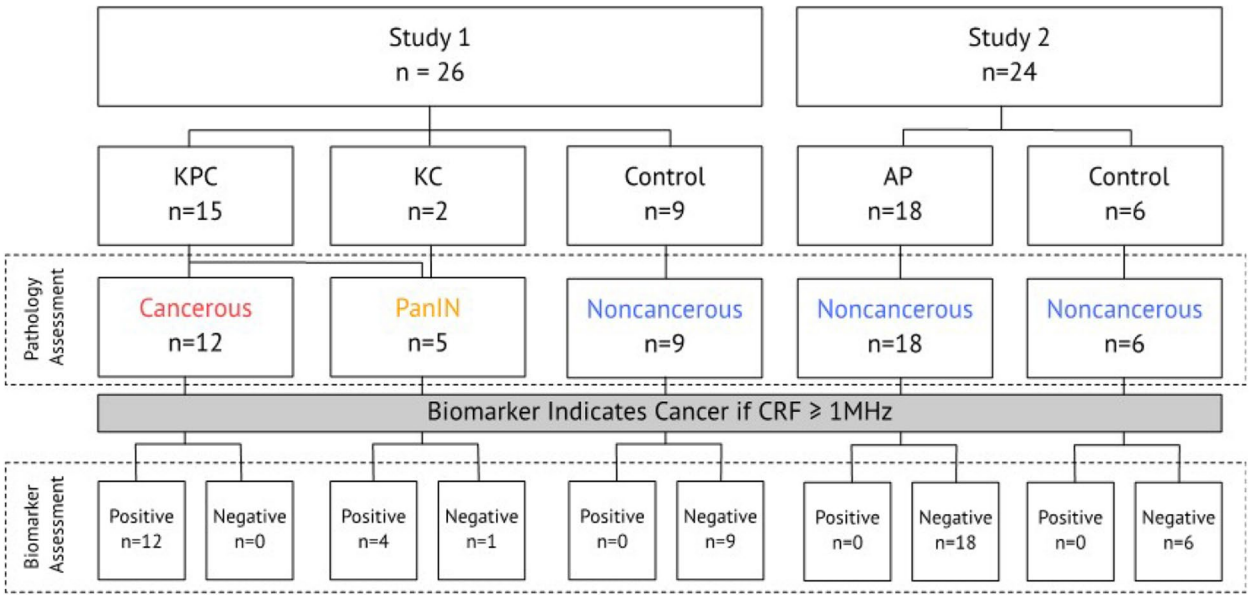

Fig. 5 Study design consisting of two double-blind studies on ex vivo pancreata of mice. In Study 1, the biomarker was tested in n=26 mice (15 KPC, 2 KC, and 9 controls), in Study 2 we determined the biomarker ability to differentiate PC from AP, considering n=24 (18 cerulein-induced AP and 6 saline-injected controls)

visually under the microscope and using QuPath) and CRF biomarker measurments. Statistical significance was set at an a-priori value of 0.01. All statistical analyses were conducted using R.

Results

In this study, we evaluated the bioimpedance-based biomarker to detect PC in genetically modified KPC and KC mouse models, acute pancreatitis (AP) mouse model and wild type controls. The KPC mouse model is one of the most widely used in vivo systems to evaluate pancreatic ductal adenocarcinoma (PDAC) due to its faithful recapitulation of human pancreatic cancer biology [33–35]. KPC PDACs provide a unique opportunity to analyze the evolution of cancer in a controlled setting, not otherwise possible in human patients. The study comprised two double-blind studies on ex vivo pancreata of mice. Study 1 involved testing the biomarker in a total of n=26 mice (15 KPC, 2 KC, and 9 controls), while Study 2 aimed to differentiate PC from AP, encompassing n=24 mice (18 cerulein-induced AP and 6 saline-injected controls) (Fig. 5).

CRF measurements were collected at various locations across the entire pancreas, and CRF determinations allowed for the calculation of sensitivity and specificity against histopathology outcomes. Regarding Study 1, based on histopathology, 12 KPC pancreases were confirmed as cancerous, 9 controls as noncancerous, while 5 pancreases (3 KPC and 2 KC) presented a precancerous condition with pancreatic intraepithelial neoplasia (PanIN). Examples of CRF curves for noncancerous, precancerous, and cancerous samples are depicted in Fig. 6.

The CRF biomarker correctly identified 4 out of 5 PanIN samples as cancerous. Considering the entire cohort of Study 1 (n=26), specificity and sensitivity were 100% and 94% respectively. Sample determinations based on the CRF biomarker are summarized in Table 1. If PanIN samples were excluded, both specificity and sensitivity were 100% (n=21).

There was a positive correlation between QuPath-estimated percent fibrosis and CRF ($F(1, 24) = 39.03$, $p < .00001$, $R2 = .62$, see Fig. 7). Percent fibrosis was also visually estimated under the microscope, showing a strong positive correlation with CRF as well ($F(1, 24) = 63.59$, $p < .00001$, $R2 = .73$, see Fig. 8)). Moreover, the percent fibrosis values estimated using the two different methods were aligned, with the QuPath estimations being consistently lower ($F(1, 24) = 79.91$, $p < .00001$, $R2 = .76$, see Fig. 9).

Discussion

This study found specificity and sensitivity of 100% and 94% respectively, of the bioimpedance-based biomarker in discerning between cancerous and noncancerous pancreas tissues from mice. Additionally, all AP samples were identified as noncancerous. These findings also determined a strong positive correlation between CRF biomarker and percent fibrosis in cancerous and

Table 1 Confusion matrix for Study 1. NC: noncancerous; CA: cancerous; PreCA: precancerous

		Histology Assessment		
		CA	**PreCA**	**NC**
NovaScan Assessment	CA	12	1	0
	PreCA	1	4	0
	NC	0	0	9

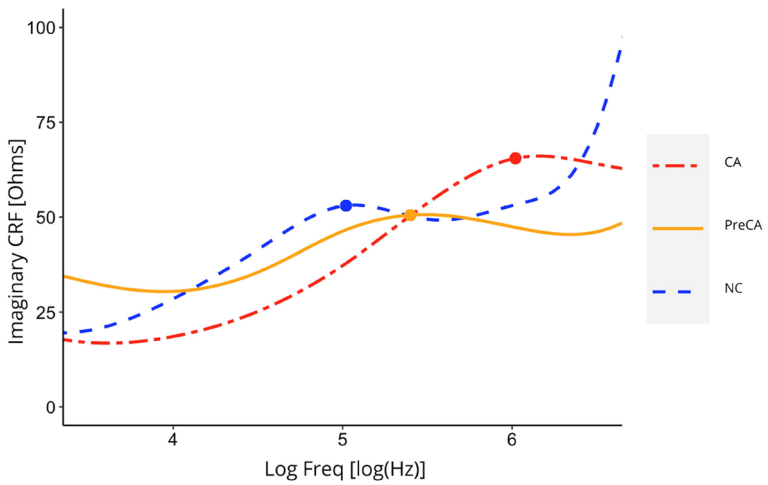

Fig. 6 Example CRF curves from noncancerous (NC - blue line), precancerous (PreCA - orange line), and cancerous (CA - red line) mice pancreases. The dashed lines indicate the frequency of the CRF peaks for each one of the curves

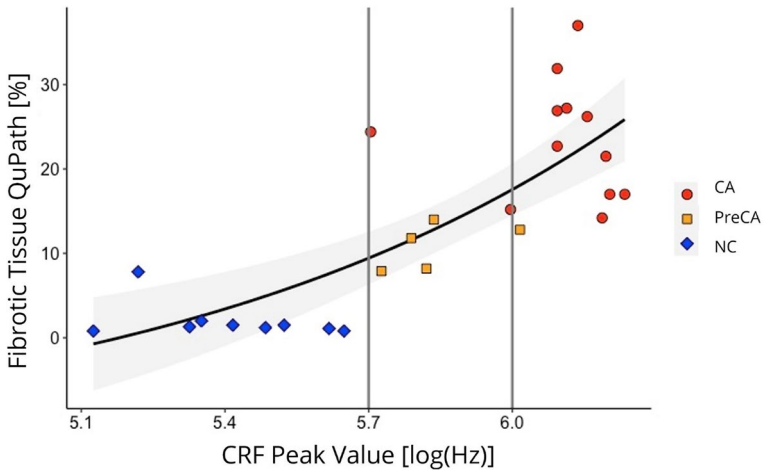

Fig. 7 Spearman correlation between percent fibrosis estimated with QuPath and CRF for noncancerous (blue), cancerous (red), and precancerous (orange) pancreases. Grey band shows the 99.99% confidence interval

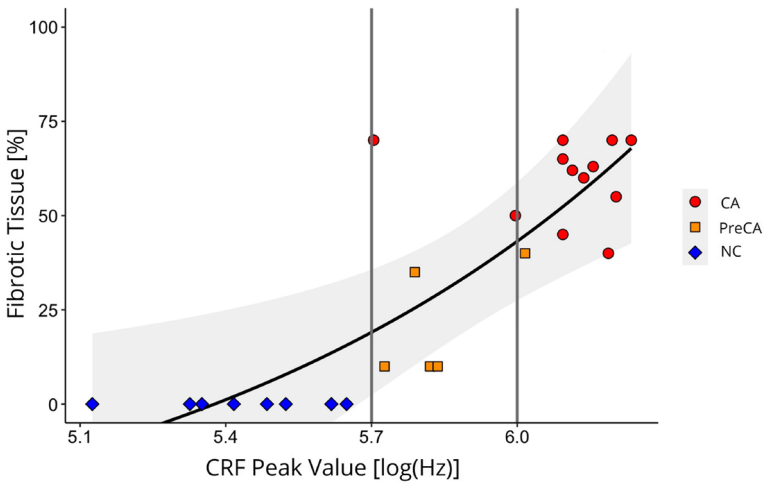

Fig. 8 Spearman correlation between percent fibrosis estimated visually under the microscope and CRF for noncancerous (blue), cancerous (red), and precancerous (orange) pancreases. Grey band shows the 99.99% confidence interval

precancerous samples. This feasibility study demonstrates the potential use of CRF in predicting PC and assessing the level of fibrosis. The identification of malignant precursors for PanIN samples indicates the biomarker's capability to detect early-stage PCs. The biomarker was found to be robust against the confounding factor of pancreatitis, demonstrating its ability to distinguish between PC, normal, and acute pancreatitis tissues, suggesting its potential clinical use in differentiating between chronic pancreatitis and PC. Indeed, future work will establish the effectiveness of CRF based technology in a commonly-employed mouse model of chronic pancreatitis.

The positive correlation between CRF biomarker and pathologically analyzed cancer-induced fibrosis in PC may be similar to that shown in breast cancer [45]. Gregory et al. [45] previously reported using the CRF biomarker as a prognostic indicator for the aggressiveness of breast cancer. In that retrospective study, a strong correlation was found between the CRF values of tumor excisions measured at time of surgery and long term patient outcomes in terms of recurrence or time-cancer-free [45]. According to their findings, when the CRF is below 5.3 log(Hz), cancer is likely non-recurrent; when the CRF ranges between 5.3 log(Hz) and 5.8 log(Hz), there is a high likelihood of recurrent cancer without metastasis; and when the CRF is above 5.8 log(Hz), there is an increasingly greater likelihood of recurrent cancer with metastasis (see Fig. 10) [45]. A similar behavior was

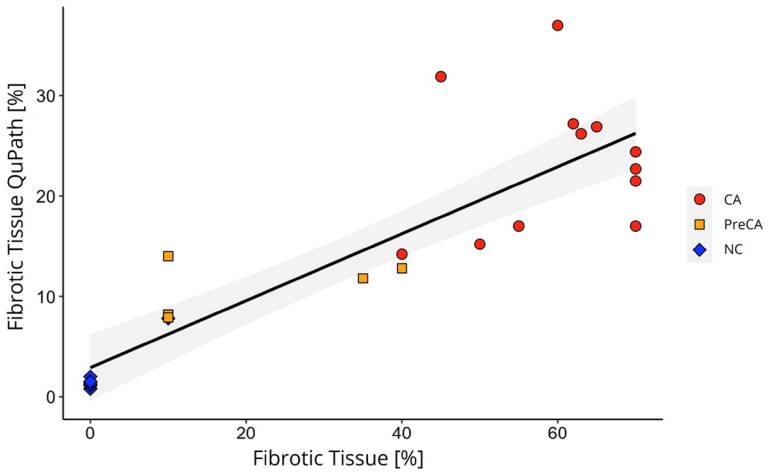

Fig. 9 Linear correlation between percent fibrosis values estimated with QuPath and visually under the microscope. Noncancerous data points are indicated in blue, cancerous in red, and precancerous in orange

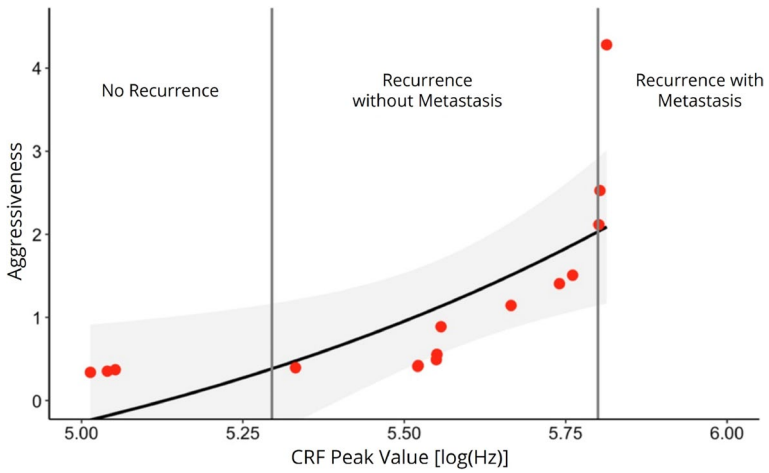

Fig. 10 Gregory et al. [45] have showed that the CRF biomarker can retrospectively classify breast cancer data in 3 well-differentiated categories: nonrecurrent; recurrent with no metastasis; and recurrent with metastasis

observed for the pacreatic tissues data presented in this currect study (see Fig. 7). These findings suggest that the CRF may be a universal property of cells, transforming regardless of organ origin, and that the CRF biomarker may serve as a prognostic indicator.

Once validated through larger preclinical and clinical trials, the CRF-based technology could be integrated into a medical device for clinical use. Specifically, the electrodes utilized for bioimpedance measurement could be refined into a digital version of Rapid On Site Evaluation (ROSE). This advanced tool would serve as an ex vivo decision support system for real-time quantitative detection of pancreatic cancer in biopsy samples obtained during endoscopic ultrasound (EUS) procedures. Adapting the technology for this purpose would require modifications to ensure its sensitivity in measuring bioimpedance for smaller sample sizes, such as biopsy specimens. ROSE offers several advantages, including timely feedback on sample adequacy, optimization of the number of needle passes performed, and potentially increased diagnostic yield [5]. However, the limited availability of on-site pathologists for ROSE poses a significant challenge, attributed to constraints related to time, personnel, and resources, thereby hindering its widespread adoption globally. The envisioned device, derived from the described technology, promises to be a more cost-effective, efficient, and accessible alternative to conventional ROSE. Its deployment would democratize the use of EUS for pancreatic cancer detection worldwide. Additionally, future developments may involve implementing

the measuring electrodes onto the tip of an endoscopic device for in vivo clinical use, aiding endoscopists in decision-making processes, facilitating margins assessment, and guiding biopsy acquisition.

This study is not without limitations. We expect some level of variability when transferring these results to a clinical trial. A larger sample size or an in vivo porcine model could provide a deeper understanding of the potential use of the biomarker for early detection of PC [55–57]. This study did not include chronic pancreatitis samples; however, a standard model for this disease is already available and will be included in a future study by this group. With this in mind, we are moving forward with developing an improved genetically altered pig model that best reflects the human condition with the primary goal of assessing CRF in combination with EUS, comparing with standard technologies that combine EUS with another modality like elastography. Once proven effective than any other approach, we propose that CRF will be a valuable and affordable tool for earlier detection of PC and are in the process of informing underserved communities for a forthcoming clinical trial, particularly in high risk individuals including African Americans with diabetes and/or pancreatitis.

Conclusions

In our research, we utilized the KPC mouse model to validate a bioimpedance-based biomarker for PC detection. Our results indicate that the CRF-based biomarker can successfully distinguish PC from pancreatitis and benign tissue. Furthermore, we observed a correlation between biomarker values and the progression of lesions from precancerous to malignant stages. These findings underscore the potential of this bioimpedance biomarker as a diagnostic tool for PC, offering promising prospects for early detection and intervention in the endoscopic field.

Abbreviations

PC	Pancreatic cancer
AP	Acute pancreatitis
CT	Computed tomography
MDCT	Multidetector computed tomography
MRI	Magnetic resonance imaging
ERCP	Endoscopic retrograde cholangiopancreatography
EUS	Endoscopic ultrasound
QE-EUS	Quantitative-elastography endoscopic ultrasound
FNA	Fine needle aspiration
FNB	Fine needle biopsy
CRF	Cole relaxation frequency
KPC	K-ras;Trp53;Pdx-1-Cre
KC	K-ras;Pdx-1-Cre
PanIN	Pancreatic intraepithelial neoplasia
PDAC	Pancreatic ductal adenocarcinoma
IP	Intraperitoneal
NC	Noncancerous
CA	Cancerous
PreCA	Precancerous
ROSE	Rapid onsite evaluation

Acknowledgements

University of Illinois at Chicago is acknowledged for providing microscopy and histopathology services.

Authors' contributions

FD, MG and LB conceived the study. FD, MG, DG and AG performed the experiments. MG, OF, DC, MJ and AG analyzed the data. CB and EK performed hardware, firmware and software technology work. KC, AC, KS, JH, JA, AJ performed vertebrate animal breeding and procedures. PG performed microscopy evaluations. AC and JH performed microscopy image analysis. FD and MG wrote the original manuscript draft. PG, IR and MG reviewed and edited the paper. All authors read and approved the final manuscript.

Funding

Not applicable.

Availability of data and materials

The datasets and codes used and/or analyzed during the current study are available from the corresponding author on reasonable request.

Declarations

Ethics approval and consent to participate

This study has been conducted in accordance with ethical standards. Studies using vertebrate animals have been performed at the University of Illinois Chicago animal core facility (under animal assurance number A3460.01). The University of Illinois Chicago is fully accredited by the Association for Assessment and Accreditation of Laboratory Animal Care (AAALAC) and operates in full compliance with all federal and state regulatory agencies.

Consent for publication

Not applicable.

Competing interests

No potential conflicts of interest were disclosed for the authors.

Received: 18 January 2024 Accepted: 14 April 2024
Published online: 03 May 2024

References

1. Globocan PS. Pancreas Statistics Globocan 2020 | WHO. 2020. https://gco.iarc.fr/today/data/factsheets/cancers/13-Pancreas-fact-sheet.pdf. Accessed 24 Nov 2023.
2. CancerStatisticsCenter. Analysis Tool | American Cancer Society - Cancer Facts & Statistics. 5-year relative survival, 2011-2017. 2022. https://cancerstatisticscenter.cancer.org/#!/data-analysis/SurvivalByStage.
3. Kato S, Honda K. Use of biomarkers and imaging for early detection of pancreatic cancer. Cancers. 2020;12(7):1965.
4. Young MR, Abrams N, Ghosh S, Rinaudo JAS, Marquez G, Srivastava S. Prediagnostic image data, artificial intelligence, and pancreatic cancer: a tell-tale sign to early detection. Pancreas. 2020;49(7):882–6.
5. Koul A, Baxi AC, Shang R, Meng X, Li L, Keilin SA, et al. The efficacy of rapid on-site evaluation during endoscopic ultrasound-guided fine needle aspiration of pancreatic masses. Gastroenterol Rep. 2018;6(1):45–8.
6. Garg SK, Chari ST. Early detection of pancreatic cancer. Curr Opin Gastroenterol. 2020;36(5):456–61.
7. Yang J, Xu R, Wang C, Qiu J, Ren B, You L. Early screening and diagnosis strategies of pancreatic cancer: a comprehensive review. Cancer Commun. 2021;41(12):1257–74.
8. Moradi F, Iagaru A. The role of positron emission tomography in pancreatic cancer and gallbladder cancer. In: Seminars in Nuclear Medicine. Elsevier; 2020;50:434–46.
9. Michl P, Löhr M, Neoptolemos JP, Capurso G, Rebours V, Malats N, et al. UEG position paper on pancreatic cancer. Bringing pancreatic cancer to the 21st century: Prevent, detect, and treat the disease earlier and better. UEG J. 2021;9(7):860–71.

10. Zhang L, Sanagapalli S, Stoita A. Challenges in diagnosis of pancreatic cancer. World J Gastroenterol. 2018;24(19):2047.
11. Arata S, Takada T, Hirata K, Yoshida M, Mayumi T, Hirota M, et al. Post-ERCP pancreatitis. J Hepato-Biliary-Pancreat Sci. 2010;17:70–8.
12. Iglesias-Garcia J, Lindkvist B, Larino-Noia J, Abdulkader-Nallib I, Dominguez-Munoz JE. Differential diagnosis of solid pancreatic masses: contrast-enhanced harmonic (CEH-EUS), quantitative-elastography (QE-EUS), or both? U Eur Gastroenterol J. 2017;5(2):236–46.
13. Dietrich C, Săftoiu A, Jenssen C. Real time elastography endoscopic ultrasound (RTE-EUS), a comprehensive review. Eur J Radiol. 2014;83(3):405–14.
14. Iordache S, Costache MI, Popescu CF, Streba CT, Cazacu S, Săftoiu A. Clinical impact of EUS elastography followed by contrast-enhanced EUS in patients with focal pancreatic masses and negative EUS-guided FNA. Med Ultrason. 2016;18(1):18–24.
15. Kitano M, Yoshida T, Itonaga M, Tamura T, Hatamaru K, Yamashita Y. Impact of endoscopic ultrasonography on diagnosis of pancreatic cancer. J Gastroenterol. 2019;54(1):19–32.
16. Varadarajulu S, Kilgore ML, Wilcox CM, Eloubeidi MA. Relationship among hospital ERCP volume, length of stay, and technical outcomes. Gastrointest Endosc. 2006;64(3):338–47.
17. Ogawa T, Kawamoto H, Harada R, Kurihara N, Kato H, Hirao K, et al. EUS-FNA is more advantageous than ERCP in tissue sampling for pathological diagnosis of pancreatic cancer. Gastrointest Endosc. 2009;69(2):S258.
18. Adamek HE, Albert J, Breer H, Weitz M, Schilling D, Riemann JF. Pancreatic cancer detection with magnetic resonance cholangiopancreatography and endoscopic retrograde cholangiopancreatography: a prospective controlled study. Lancet. 2000;356(9225):190–3.
19. Chang KJ, Nguyen P, Erickson RA, Durbin TE, Katz KD. The clinical utility of endoscopic ultrasound-guided fine-needle aspiration in the diagnosisand staging of pancreatic carcinoma. Gastrointest Endosc. 1997;45(5):387–93.
20. Varadarajulu S, Wallace MB. Applications of endoscopic ultrasonography in pancreatic cancer. Cancer Control. 2004;11(1):15–22.
21. Bispo M, Marques S, Rio-Tinto R, Fidalgo P, Devière J. The role of endoscopic ultrasound in pancreatic cancer staging in the Era of neoadjuvant therapy and personalised medicine. GE-Port J Gastroenterol. 2021;28(2):111–20.
22. Shrikhande SV, Barreto SG, Goel M, Arya S. Multimodality imaging of pancreatic ductal adenocarcinoma: a review of the literature. HPB. 2012;14(10):658–68.
23. Wang W, Shpaner A, Krishna SG, Ross WA, Bhutani MS, Tamm EP, et al. Use of EUS-FNA in diagnosing pancreatic neoplasm without a definitive mass on CT. Gastrointest Endosc. 2013;78(1):73–80.
24. DeWitt J, Devereaux B, Chriswell M, McGreevy K, Howard T, Imperiale TF, et al. Comparison of endoscopic ultrasonography and multidetector computed tomography for detecting and staging pancreatic cancer. Ann Intern Med. 2004;141(10):753–63.
25. Pritchett MA, D Duke J, Williams J, Schirmer C, D Sturgis C, Hartley C, et al. Automated sample preparation system for endobronchial ultrasound (EBUS): ROSE APPLICATIONS. Chest. 2022;162(4):A1863–4.
26. Duke, Jennifer D., Charles D. Sturgis, Christopher Hartley, Morgan Bailey, Michal Reid, Ryan Kern, Alex Bluestone, Hariharan Subramanian, and Janani Reisenauer. Evaluation of automated sample preparation system for lymph node sampling. J Thorac Dis. 2023;15(8):4229.
27. Sans M, Zhang J, Lin JQ, Feider CL, Giese N, Breen MT, et al. Performance of the MasSpec Pen for rapid diagnosis of ovarian cancer. Clin Chem. 2019;65(5):674–83.
28. Jain M, Robinson BD, Salamoon B, Thouvenin O, Boccara C, Mukherjee S. Rapid evaluation of fresh ex vivo kidney tissue with full-field optical coherence tomography. J Pathol Inform. 2015;6(1):53.
29. Gregory W, Marx J, Gregory C, Mikkelson W, Tjoe J, Shell J. The Cole relaxation frequency as a parameter to identify cancer in breast tissue. Med Phys. 2012;39(7Part1):4167–74.
30. Svoboda RM, Gharia MJ, Shell J, Gregory WD. Bioimpedance measurement as an assessment of margin positivity in Mohs surgical specimens of nonmelanoma skin cancer: Management implications. J Am Acad Dermatol. 2018;79(3):591–3.
31. Bogdanowicz L, Fidaner O, Ceres D, Grycuk A, Guidetti M, Demos D, et al. The Cole Relaxation Frequency as a Parameter to Identify Cancer in Lung Tissue: Preliminary Animal and Ex Vivo Patient Studies. Biomed Eng. 2022;7(1):e35346.
32. Guidetti M, Bogdanowicz L, Fidaner O, Ceres D, Grycuk A, Gehrke DS, et al. Cole relaxation frequency: a parameter to assess lymph node status in patients with lung cancer. Chest. 2022;162(4):A1659–60.
33. Hu S, Pan L, Shangguan J, Figini M, Eresen A, Sun C, et al. Non-invasive dynamic monitoring initiation and growth of pancreatic tumor in the LSL-KrasG12D/+; LSL-Trp53R172H/+; Pdx-1-Cre (KPC) transgenic mouse model. J Immunol Methods. 2019;465:1–6.
34. Renz BW, Takahashi R, Tanaka T, Macchini M, Hayakawa Y, Dantes Z, et al. β2 adrenergic-neurotrophin feedforward loop promotes pancreatic cancer. Cancer Cell. 2018;33(1):75–90.
35. Niknafs N, Zhong Y, Moral JA, Zhang L, Shao MX, Lo A, et al. Characterization of genetic subclonal evolution in pancreatic cancer mouse models. Nat Commun. 2019;10(1):1–10.
36. Mishra V, Bouayad H, Schned A, Hartov A, Heaney J, Halter RJ. A real-time electrical impedance sensing biopsy needle. IEEE Trans Biomed Eng. 2012;59(12):3327–36.
37. Mahara A, Khan S, Murphy EK, Schned AR, Hyams ES, Halter RJ. 3D microendoscopic electrical impedance tomography for margin assessment during robot-assisted laparoscopic prostatectomy. IEEE Trans Med Imaging. 2015;34(7):1590–601.
38. Halter RJ, Hartov A, Poplack SP, Wells WA, Rosenkranz KM, Barth RJ, et al. Real-time electrical impedance variations in women with and without breast cancer. IEEE Trans Med Imaging. 2014;34(1):38–48.
39. Halter RJ, Hartov A, Heaney JA, Paulsen KD, Schned AR. Electrical impedance spectroscopy of the human prostate. IEEE Trans Biomed Eng. 2007;54(7):1321–7.
40. Qiao G, Duan W, Chatwin C, Sinclair A, Wang W. Electrical properties of breast cancer cells from impedance measurement of cell suspensions. In: Journal of Physics: conference series. vol. 224. IOP Publishing; 2010. p. 012081.
41. Han A, Yang L, Frazier AB. Quantification of the heterogeneity in breast cancer cell lines using whole-cell impedance spectroscopy. Clin Cancer Res. 2007;13(1):139–43.
42. Shell J, Gregory WD. Efficient cancer detection using multiple neural networks. IEEE J Transl Eng Health Med. 2017;5:1–7.
43. Gabriel S, Lau R, Gabriel C. The dielectric properties of biological tissues: III. Parametric models for the dielectric spectrum of tissues. Phys Med Biol. 1996;41(11):2271.
44. Cole KS, Cole RH. Dispersion and absorption in dielectrics I. Alternating current characteristics J Chem Phys. 1941;9(4):341–51.
45. Gregory WD, Christie SM, Shell J, Nahhas GJ, Singh M, Mikkelson W. Cole relaxation frequency as a prognostic parameter for breast cancer. J Patient-Centered Res Rev. 2020;7(4):343.
46. Subramanian H, Roy HK, Pradhan P, Goldberg MJ, Muldoon J, Brand RE, et al. Nanoscale cellular changes in field carcinogenesis detected by partial wave spectroscopy. Cancer Res. 2009;69(13):5357–63.
47. Hingorani SR, Petricoin EF, Maitra A, Rajapakse V, King C, Jacobetz MA, et al. Preinvasive and invasive ductal pancreatic cancer and its early detection in the mouse. Cancer Cell. 2004;5(1):103.
48. Hingorani SR, Wang L, Multani AS, Combs C, Deramaudt TB, Hruban RH, et al. Trp53R172H and KrasG12D cooperate to promote chromosomal instability and widely metastatic pancreatic ductal adenocarcinoma in mice. Cancer Cell. 2005;7(5):469–83.
49. Gabriel ANA, Jiao Q, Yvette U, Yang X, Al-Ameri SA, Du L, et al. Differences between KC and KPC pancreatic ductal adenocarcinoma mice models, in terms of their modeling biology and their clinical relevance. Pancreatology. 2020;20(1):79–88.
50. Vernucci E, Abrego J, Gunda V, Shukla SK, Dasgupta A, Rai V, et al. Metabolic alterations in pancreatic cancer progression. Cancers. 2019;12(1):2.
51. Hingorani SR, Petricoin EF, Maitra A, Rajapakse V, King C, Jacobetz MA, et al. Preinvasive and invasive ductal pancreatic cancer and its early detection in the mouse. Cancer Cell. 2003;4(6):437–50.
52. Drosos Y, Escobar D, Chiang MY, Roys K, Valentine V, Valentine MB, et al. ATM-deficiency increases genomic instability and metastatic potential in a mouse model of pancreatic cancer. Sci Rep. 2017;7(1):11144.
53. Bombardo M, Malagola E, Chen R, Rudnicka A, Graf R, Sonda S. Ibuprofen and diclofenac treatments reduce proliferation of pancreatic acinar cells upon inflammatory injury and mitogenic stimulation. Br J Pharmacol. 2018;175(2):335–47.

54. O'Brien BJ, Faraoni EY, Strickland LN, Ma Z, Mota V, Mota S, Chen X, et al. CD73-generated extracellular adenosine promotes resolution of neutrophil-mediated tissue injury andrestrains metaplasia in pancreatitis. The FASEB Journal. 2023;37:1.
55. Principe DR, Overgaard NH, Park AJ, Diaz AM, Torres C, McKinney R, et al. KRASG12D and TP53R167H cooperate to induce pancreatic ductal adenocarcinoma in sus scrofa pigs. Sci Rep. 2018;8(1):12548.
56. Bailey KL, Carlson MA. Porcine models of pancreatic cancer. Front Oncol. 2019;9:144.
57. Bailey KL, Cartwright SB, Patel NS, Remmers N, Lazenby AJ, Hollingsworth MA, et al. Porcine pancreatic ductal epithelial cells transformed with KRASG12D and SV40T are tumorigenic. Sci Rep. 2021;11(1):13436.

Publisher's Note